Roll Angle Estimation Algorithm for a Spinning Vehicle on a Ballistic Trajectory Based on MEMS Gyroscope Data

I.L. Surov[a] and K.S. Alekseeva[b]*

[a]Gyrooptics, St. Petersburg, Russia
[b]Baltic State Technical University Voenmech, St. Petersburg, Russia
e-mail: pestova.ksu@gmail.com
Received September 29, 2023; reviewed March 5, 2024; accepted April 10, 2024

Abstract: The paper describes an algorithm of in-flight roll angle estimation for a spinning vehicle following an unguided trajectory based on MEMS gyroscope triad data. The roll angles are estimated with a phase detector by demodulating the signals of transverse gyroscopes with subsequent least squares processing.

Keywords: roll angle, spinning vehicle, phase detector, micromechanical gyroscopes, ballistic trajectory.

1. INTRODUCTION

In fast spinning vehicle technology, the major problem is to generate the precise roll angle and to reduce the scale factor error for the longitudinal gyroscope (angular rate sensor) [1, 11]. For these vehicles, the roll error can be unacceptably large, which can lead to the loss of control. Due to high longitudinal angular velocity, the longitudinal gyroscope scale factor greatly contributes to the navigation system error. To provide the precise navigation solution, the gyroscope scale factor should be additionally corrected during the motion.

Avionics of these vehicles is commonly activated during the motion. Before running the inertial navigation system algorithms, its initial alignment, particularly roll alignment, should be performed. For a vehicle following a ballistic trajectory, the initial projections of the linear velocity, coordinates, and yaw and pitch angles can be determined if its motion equations are known. External navigation aids can also be applied, such as GNSS receivers, whose readiness time is sever-al seconds in the warm start mode. The roll angle, however, cannot be estimated in this way. The paper considers in-flight determination of the initial phase and estimation of the current roll angle.

There are the following methods to determine the initial phase and reduce the roll error for this vehicle type:

- isolating the IMU (inertial measurement unit) from rotation about the longitudinal axis with the vehicle body [1];

- applying an additional single-axis gyrostabilizer on the longitudinal axis [1, 2];

- employing non-inertial measurements such as data from magnetometers [3–5], GNSS phase measurements [4, 6], optical sensors [7], pirometric sensors [8], signal zero-crossing tags [1], etc.;

- forced precession and estimation of its parameters using accelerometers in-stalled on the vehicle in a special manner [1];

- improving the observability of attitude errors by shifting the accelerometers from the rotation axis [9, 10], non-orthogonal installation of the sensitivity axes [9, 11] or installation at an angle to the rotation axis [11, 12].

Applying external velocity and position measurements for correcting the analytical vertical does not always prove effective, because on the ballistic trajectory the specific force of the vehicle center of mass is determined mostly by the drag force and forms the measurement along the vehicle longitudinal axis, while the measurements on transverse axes are close to zero.

In this article the roll angle for a spinning vehicle is determined algorithmically, that is, no additional sensors or design solutions have been used.

The stated problem can be algorithmically solved using

- special attitude determination algorithms [12–15], which, however, cannot be used to perform the initial alignment, particularly, to determine the roll angle initial phase;

- dynamics equations of center of mass and aerodynamic parameters of the vehicle [16, 17];

- methods of correcting the roll angle with account for the specific motion of the rotation-stabilized vehicle [18–24].

An algorithm of strapdown inertial navigation system (SINS) operation pro-posed in [18] relies on the known initial alignment data. However, this functioning principle of the navigation system is not always feasible and is not suitable for the considered problem.

In [19], the roll angles are estimated using the rates of change of heading and elevation angles, which are determined as the projections on the stability reference frame with account for the ballistic motion or GNSS data. This approach assumes that the pitch angle is small. As an example, vehicle rotation about the longitudinal axis at a constant frequency of max 2 Hz is considered.

In [20], the roll angles are determined using the Kalman filter, relying on [19], and additionally estimate the longitudinal angular velocity and biases of the transverse gyroscopes. Similarly to [19], this algorithm assumes small pitch angles, which can introduce large errors in the roll angle estimation.

In [21], the roll angle is found using the phase of the estimated pitch and yaw angles and the integral of the vehicle yawing rate. It should be noted, however, that this algorithm features large errors in conditions of noisy gyroscope signals, systematic errors, high rotation rate, and low-frequency signal processing.

In [22–24], the roll estimation algorithm uses the phase detector based on demodulation of transverse gyroscope signals. A complementary filter [15] is applied after demodulation in [22, 23]. These publications do not consider the scale factor error of the longitudinal gyroscope and yaw rate correction.

In this paper we focus on current roll angle estimation for a fast spinning vehicle using the MEMS gyroscope triad calibrated in the range of the measured angular velocities and environment temperatures and collinear with the axes of the body frame. A gyroscope with broad dynamic range is installed on the longitudinal axis for measuring the projections of the angular velocity vector. The reference trajectory is ballistic and lies within the atmosphere. The roll angle estimation algorithm is activated at the flight right after initializing the onboard avionics and runs until the GNSS receiver data are ready and SINS algorithm starts.

The algorithm is intended to estimate the current roll angle and the scale factor error of a longitudinal gyroscope with its further in-flight recalibration. This is done using the modulation of the transverse gyroscope signals at the rotation frequency on the initial unguided part of the ballistic trajectory.

The mathematical model of the studied process is described, and a roll angle estimation algorithm for undisturbed measurements is proposed. The algorithm modification using MEMS gyroscope triad is proposed. The algorithm simulation results for six reference trajectories are provided with account for the typical errors and measurement noise.

2. DESCRIPTION OF THE MATHEMATICAL MODEL

Denote the launching frame by $OX_cY_cZ_c$, stability frame, by $OX_eY_eZ_e$, and body frame, as $OXYZ$, where OX_cY_c is the firing plane. The frames are defined according to GOST 20058-80. The stability frame has its origin at the vehicle center of mass, axis OX_e coincides with the longitudinal body axis OX, axis OY_e is perpendicular to OX_e and lies in the vertical plane passing through OX, and axis OZ_e complements the system to the right-hand frame. The stability frame has two degrees of freedom of the rotational motion.

The vehicle has a short flight time, so the launching frame rotation velocity relative to the inertial frame is considered to be negligibly small.

According to the kinematic equation of the vehicle rotational motion, the roll angle γ is determined as follows:

$$\gamma(t) = \int_0^t \left(\omega_x - \mathrm{tg}(\vartheta) \cdot \left(\omega_y \cdot \cos(\gamma) - \omega_z \cdot \sin(\gamma)\right)\right) dt + \gamma_0, \quad (1)$$

where ω_x, ω_y, ω_z are the projections of the vehicle absolute angular velocity on the body frame axes, measured with the gyroscopes with no instrumental measurement errors, rad/s; ϑ is the pitch angle, rad; γ_0 is the initial roll angle, rad.

To estimate the current roll angle, its initial phase γ_0 should be found. The estimate of γ_0 is generated

using the phase detector algorithm with the modulation of the signals of transverse gyroscopes.

Projections of the vehicle absolute angular velocity on the axes OY_e and OZ_e of the stability frame are modulated with the roll angle, which provides the projections on the axes OY and OZ of the body frame. They are measured by the transverse gyroscopes in the absence of instrumental measurement errors:

$$\omega_y = \omega_{ye} \cdot \cos(\gamma) + \omega_{ze} \cdot \sin(\gamma),$$
$$\omega_z = -\omega_{ye} \cdot \sin(\gamma) + \omega_{ze} \cdot \cos(\gamma), \qquad (2)$$

where ω_{ye}, ω_{ze} are the projections of the vehicle absolute angular velocity on the stability axes, rad/s.

For the demodulation procedure, we define the angle γ_a as the integral of the projection of the vehicle absolute angular velocity on the longitudinal body axis:

$$\gamma_a(t) = \int_0^t \omega_x dt. \qquad (3)$$

The intermediate value of the angle γ_a is an auxiliary value, which is not actually the roll angle. It can be interpreted as the roll value when assuming a small change in the yaw angle $\dot\psi \approx 0$ and a zero initial phase.

Demodulating the projections ω_y and ω_z is performed according to the formulas:

$$v_1 = \omega_z \cdot \sin(\gamma_a) - \omega_y \cdot \cos(\gamma_a),$$
$$v_2 = \omega_y \cdot \sin(\gamma_a) + \omega_z \cdot \cos(\gamma_a). \qquad (4)$$

Substituting (2) to (4) and applying the trigonometric formulas for the product transformation yields

$$v_1 = -\omega_{ye} \cdot \cos(\gamma - \gamma_a) - \omega_{ze} \cdot \sin(\gamma - \gamma_a),$$
$$v_2 = -\omega_{ye} \cdot \sin(\gamma - \gamma_a) + \omega_{ze} \cdot \cos(\gamma - \gamma_a). \qquad (5)$$

If the current roll angle is represented as the product of the average angular velocity by time

$$\gamma = \overline{\omega}_x \cdot t + \gamma_0,$$
$$\gamma_a = \overline{\omega}_a \cdot t, \qquad (6)$$

where $\overline{\omega}_x$ and $\overline{\omega}_a$ are the average angular velocities over time t, rad; then with close $\overline{\omega}_x$ and $\overline{\omega}_a$ the harmonic signals caused by the angle difference have a low frequency $\Delta\omega = \overline{\omega}_x - \overline{\omega}_a$.

To exclude high-frequency components, the generated v_1 and v_2 pass a low-pass filter:

$$v_{1LPF}(s) = W_{LPF}(s) \cdot v_1(s),$$

$$v_{2LPF}(s) = W_{LPF}(s) \cdot v_2(s). \qquad (7)$$

As a result of filtering, the output values contain low-frequency terms with account for the filter gain k_{LPF}:

$$v_{1LPF} = -k_{LPF} \cdot \omega_{ye} \cdot \cos(\gamma - \gamma_a) - k_{LPF} \cdot \omega_{ze} \cdot \sin(\gamma - \gamma_a),$$
$$v_{2LPF} = -k_{LPF} \cdot \omega_{ye} \cdot \sin(\gamma - \gamma_a) + k_{LPF} \cdot \omega_{ze} \cdot \cos(\gamma - \gamma_a). \qquad (8)$$

Transforming (8) provides

$$\frac{v_{1LPF}}{k_{LPF} \cdot \sqrt{\omega_{ye}^2 + \omega_{ze}^2}} =$$
$$= -\frac{\omega_{ye}}{\sqrt{\omega_{ye}^2 + \omega_{ze}^2}} \cdot \cos(\gamma - \gamma_a) - \frac{\omega_{ze}}{\sqrt{\omega_{ye}^2 + \omega_{ze}^2}} \cdot \sin(\gamma - \gamma_a).$$

Derive the angle β, for which

$$\sin\beta = \frac{\omega_{ye}}{\sqrt{\omega_{ye}^2 + \omega_{ze}^2}}, \cos\beta = \frac{\omega_{ze}}{\sqrt{\omega_{ye}^2 + \omega_{ze}^2}},$$

then

$$\frac{v_{1LPF}}{k_{LPF} \cdot \sqrt{\omega_{ye}^2 + \omega_{ze}^2}} = -\sin(\beta + \gamma - \gamma_a). \qquad (9)$$

Similarly,

$$\frac{v_{2LPF}}{k_{LPF} \cdot \sqrt{\omega_{ye}^2 + \omega_{ze}^2}} = \cos(\beta + \gamma - \gamma_a), \qquad (10)$$

hence

$$\frac{v_{1LPF}}{v_{2LPF}} = -\mathrm{tg}(\beta + \gamma - \gamma_a). \qquad (11)$$

Then, with account for (6), the argument of tangent function can be presented as

$$\gamma - \gamma_a + \beta = \Delta\omega \cdot t + \gamma_0 + \beta, \qquad (12)$$

hence

$$\Delta\omega \cdot t + \gamma_0 + \beta + \pi \cdot n = -\mathrm{atan}\left(\frac{v_{1LPF}}{v_{2LPF}}\right), n \in Z. \qquad (13)$$

The arctangent function is determined with two arguments, which allows calculating the quadrant of the result in the range $[0; 2\pi]$ and eliminate the uncertainty of the term $\pi \times n$, $n \in Z$ from (13). This term will then be omitted.

Present $\Delta\omega$ in the form

$$\Delta\omega = \overline{\omega}_a \cdot \left(\frac{\overline{\omega}_x}{\overline{\omega}_a} - 1\right), \qquad (14)$$

hence

$$\gamma_a \cdot \left(\frac{\overline{\omega}_x}{\overline{\omega}_a} - 1\right) + \gamma_0 + \beta = -\text{atan}\left(\frac{v_{1LPF}}{v_{2LPF}}\right). \quad (15)$$

The theoretical algorithm of the phase detector, described by (4)-(15), is implemented using the gyro measurements containing the errors.

The angle γ_a is estimated by numerical integration of (3) with account for the longitudinal gyroscope data $\omega_{x\Pi}$ under zero initial conditions:

$$\hat{\gamma}_a(t) = \int_0^t \omega_{x\Pi} dt. \quad (16)$$

When processing the transverse gyroscope signals, the data pass a bandpass filter with a second-order characteristic equation to isolate the signal components at the spinning frequency. The filter central frequency is adjusted depending on the rotation frequency. The bandpass filter transfer function can be written as

$$W_{BPF}(s) = \frac{\dfrac{\omega_0}{Q} \cdot s}{s^2 + \dfrac{\omega_0}{Q} \cdot s + \omega_0^2}, \quad (17)$$

where ω_0 is the filter central frequency; $Q = \omega_0 / (2 \cdot \pi \cdot \Delta f)$ is the filter Q-factor for the given filter bandwidth Δf. This value is conditioned by the frequency characteristics of the gyroscopes used in the algorithm.

To obtain a discrete filter with the specified cutoff frequencies, the cutoff frequencies of the analog model should be corrected to compensate for the distortion of the frequency axis:

$$\omega_0 = \frac{2}{T_s} \cdot \text{tg}\left(\omega_{x\Pi} \cdot \frac{T_s}{2}\right). \quad (18)$$

Bilinear transformation provides the equation for the digital filter

$$W_{BPF}(z) = \frac{\dfrac{b_0}{a_0} + \dfrac{b_1}{a_0} z^{-1} + \dfrac{b_2}{a_0} z^{-2}}{1 + \dfrac{a_1}{a_0} z^{-1} + \dfrac{a_2}{a_0} z^{-2}} \quad (19)$$

with the coefficients $a_0 = 4 \cdot Q + 2 \cdot T_s \cdot \omega_0 + Q \cdot T_s^2 \cdot \omega_0^2$, $a_1 = -8 \cdot Q + 2 \cdot Q \cdot T_s^2 \cdot \omega_0^2$, $a_2 = 4 \cdot Q - 2 \cdot T_s \cdot \omega_0 + Q \cdot T_s^2 \cdot \omega_0^2$, $b_0 = 2 \cdot T_s \cdot \omega_0$, $b_1 = 0$, $b_2 = -2 \cdot T_s \cdot \omega_0$, where T_s is the input data sampling period. The filter is adjusted depending on the current $\omega_{x\Pi}$ at the gyroscope readout frequency.

The phase detector is realized using the estimated angle $\hat{\gamma}_a(t)$ and the signals of the transverse gyroscopes $w_{yy\Pi 1}$ and $w_{zz\Pi 1}$, passed through the digital filter (19). To do this, the demodulator estimates the auxiliary values v_{v1} and v_{v2} according to (4):

$$\hat{v}_1 = \omega_{z\Pi 1} \cdot \sin(\hat{\gamma}_a) - \omega_{y\Pi 1} \cdot \cos(\hat{\gamma}_a),$$
$$\hat{v}_2 = \omega_{y\Pi 1} \cdot \sin(\hat{\gamma}_a) + \omega_{z\Pi 1} \cdot \cos(\hat{\gamma}_a). \quad (20)$$

The generated estimates $\hat{v}_1$ and $\hat{v}_2$ are passed through the digital low-pass filter to exclude the high-frequency components according to (7). The filter is selected based on the cutoff frequency, which is a compromise between the required filter speed and resistance to typical fluctuations, and the typical scale factor error of the longitudinal gyroscope. The known phase shift of the filter should be taken into account in the term Δ_{ylpf}, added to the result obtained using the algorithm for detecting the initial phase of the roll angle.

The least squares method (LSM) is implemented for the linear regression using the estimated angle $\hat{\gamma}_a$, estimates $\hat{v}_{1LPF}$, $\hat{v}_{2LPF}$ with account for (15)

$$\hat{\gamma}_a \cdot k_{LSM} + b_{LSM} = -\text{atan}\left(\frac{\hat{v}_{1LPF}}{\hat{v}_{2LPF}}\right), \quad (21)$$

where k_{LSM}, b_{LSM} are the linear regression coefficients:

$$k_{LSM} = \left(\frac{\overline{\omega}_x}{\overline{\omega}_a} - 1\right), b_{LSM} = \gamma_0 + \beta. \quad (22)$$

The coefficient k_{LSM} estimates the scale factor error of the longitudinal gyroscope, which is further corrected during the flight according to the equation

$$\hat{\omega}_{x\Pi} = \omega_{x\Pi} + k_{\text{мнк}} \cdot \omega_{x\Pi}. \quad (23)$$

With account for the equality (12), the current roll angle $\hat{\gamma}$ is estimated using

$$\hat{\gamma} = \hat{\gamma}_a \cdot (k_{\text{мнк}} + 1) + b_{\text{мнк}} - \beta + \Delta\gamma_{lpf}. \quad (24)$$

The correction $\Delta\gamma_{lpf}$ is determined as a phase delay of the applied low-pass filter at frequency $\Delta\omega$. The correction β is found as follows:

$$\beta = \begin{cases} \text{atan}\left(\dfrac{\omega_{ye}}{\omega_{ze}}\right), \text{if } \omega_{ze} > 0 \\ \pi + \text{atan}\left(\dfrac{\omega_{ye}}{\omega_{ze}}\right), \text{if } \omega_{ze} < 0 \end{cases} = \begin{cases} \text{atan}\left(\dfrac{\dot{\psi}\cos\vartheta}{\dot{\vartheta}}\right), \text{if } \dot{\vartheta} > 0, \\ \pi + \text{atan}\left(\dfrac{\dot{\psi}\cos\vartheta}{\dot{\vartheta}}\right), \text{if } \dot{\vartheta} < 0. \end{cases}$$
$$(25)$$

By analogy with (15), the arctangent is found using two arguments in the range $[0; 2\pi]$, which allows avoiding the "if" condition.

Numerical values of ψ, $\dot{\vartheta}$, and ϑ can be calculated with the initial alignment algorithm using a reference trajectory or a simplified vehicle motion model within a short time interval of about a few seconds, where the roll angle estimation algorithm performs properly. If no initial alignment data are available, we take $\beta = 0$ (at $\dot{\vartheta} > 0$) or $\beta = \pi$ (at $\dot{\vartheta} < 0$), depending on the vehicle motion type.

3. SIMULATION RESULTS

The roll angle estimation algorithm was tested on reference data obtained by simulating the motion of a rotation-stabilized vehicle for six different trajectories in a deterministic formulation (Figs. 1–2).
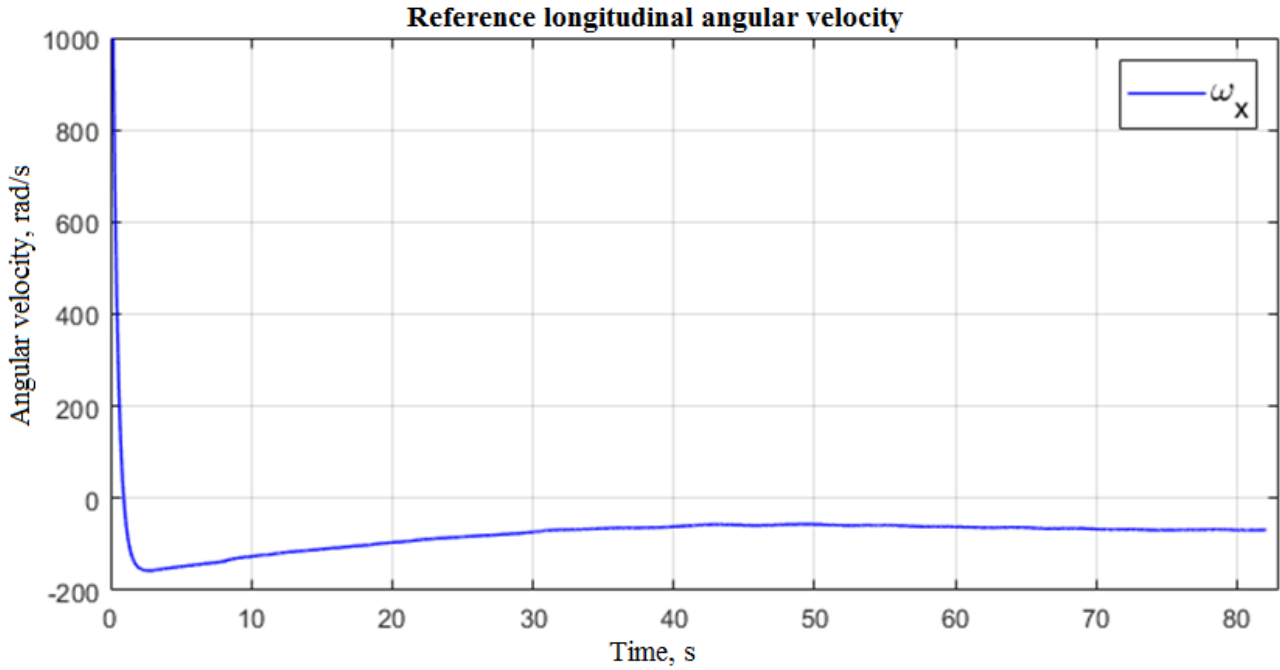
Fig. 1. Reference longitudinal angular velocity for trajectory 1.
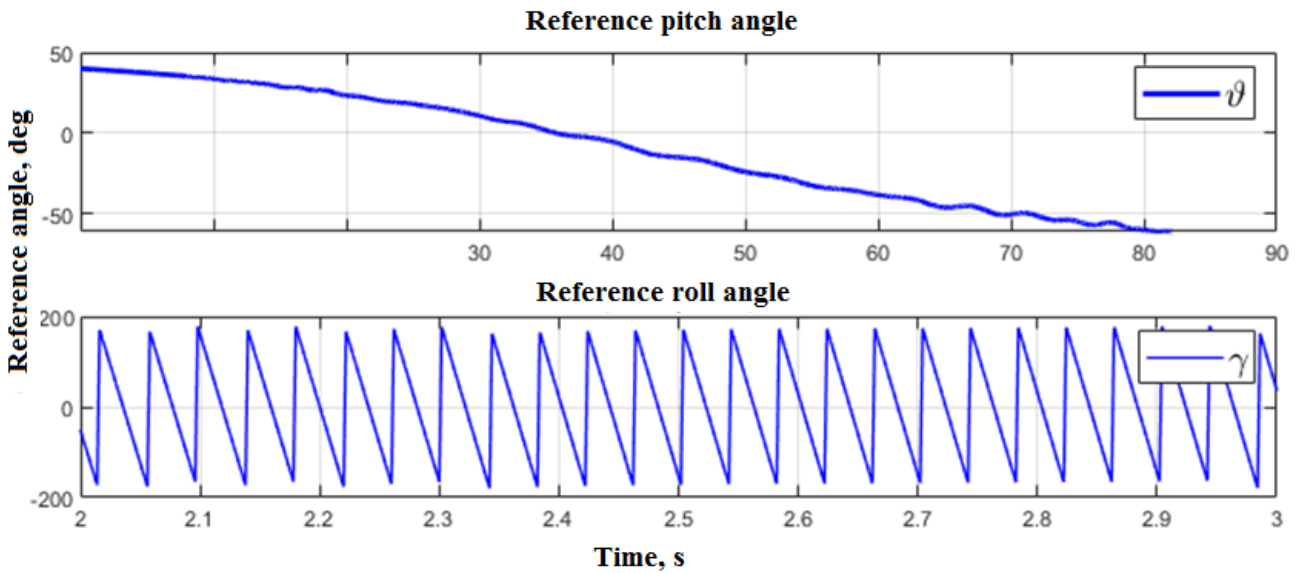
Fig. 2. Reference pitch and roll angles for trajectory 1.

The reference angular velocities for each trajectory are the input data for simulating the gyroscope signals being the sum of the useful signal, systematic and random errors. The accepted sensor errors are presented in Table. 1, where $N(m; \sigma^2)$ is a normally distributed random variable with the mathematical expectation m and root-mean-square deviation σ.

Table 1. Numerical values of gyroscope errors.

Parameter, dimensions	Value
Bias at the start, deg/s	$N(0; 0,1^2)$
Scale factor error, %	$N(0; 0.033^2)$
Bias instability, deg/s	$2.5 \cdot 10^{-3}$
Angular random walk, (deg/s)·√s	$2 \cdot 10^{-3}$
Quantization error, deg	$0.75 \cdot 10^{-3}$
Velocity random walk, (deg/s)·√s	$2 \cdot 10^{-4}$
Linear drift of the output signal, (deg/s^2)·deg/√s	$N(0; (0.2 \cdot 10^{-3})^2)$
Misalignment angles between the gyroscope and body frames, deg	$N(0; (0.033)^2)$

The obtained gyroscope signal passes the transfer function to generate the sensor dynamic errors and the required frequency characteristics. The gyroscope transfer function is formed as a sequence of the following links:

- oscillatory link considering the gyroscope dynamics;
- compensation of the oscillatory link, that is, nonideal reduction with account for the deviation of the natural frequency and Q-factor;
- second-order low-pass filter with a natural frequency 225 Hz and a Q-factor $Q = 1$;
- filter averaging the frequency to the update rate;
- ideal delay for one output update period.

The simulation starts at $t_{t1} = 2.5$ s (with account for the readiness time of the onboard electronic equipment) and continues till $t_{t2} = 8$ s, when the vehicle motion control begins. The reference data are sampled and processed at $f_{fs} = 500$ Hz. The roll angle error $\Delta\gamma$, obtained by comparing with the reference angles in the deterministic formulation, is shown in Fig. 3. The plots present the roll angle error vs. time since 4.5 s to exclude the filters' and LSM convergence periods.

Figure 4 presents the scale factor error estimate compared to the preset systematic scale factor error of the longitudinal gyroscope.
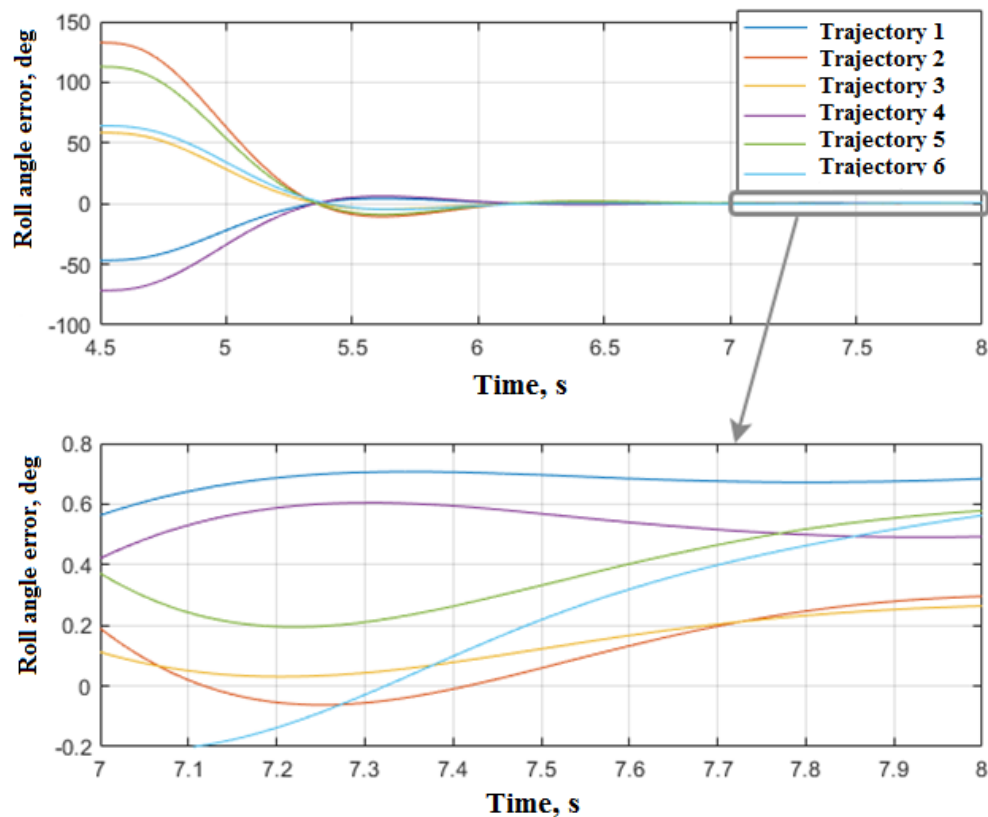
Fig. 3. Roll angle errors
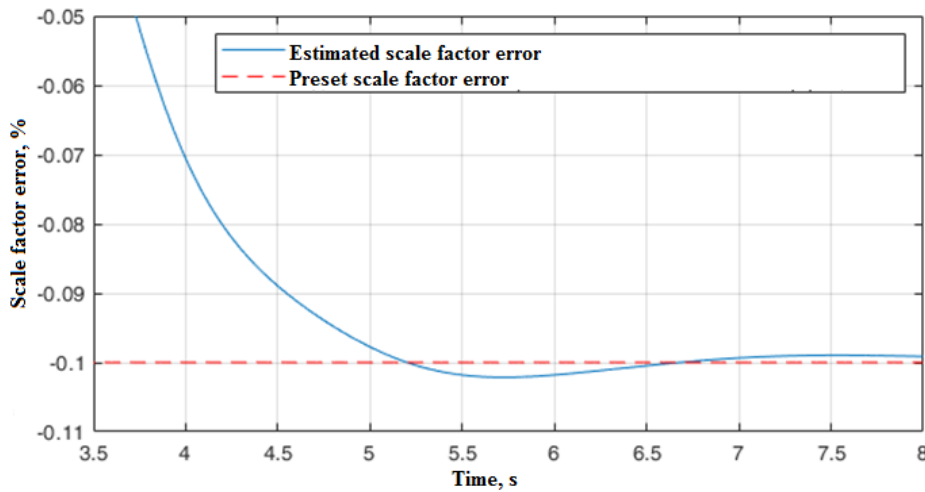
Fig. 4. Estimate of scale factor error for the longitudinal gyroscope.

Statistical characteristics of the roll angle error $\Delta\gamma$ have been calculated with account for the gyroscope errors in the stochastic formulation. Five hundred simulation runs of the algorithm were made and the obtained set of numerical values of the roll errors at time t_2 was statistically processed. As statistical indicators, we used the mathematical expectation (ME), RMS deviation, and 2.5 percentile and 97.5 percentile, which specify the boundaries of the interval (IB) containing 95% of observations and determine the normal peak-to-peak range.

Table 2.
Statistical characteristics of roll angle error without correcting the gyroscope scale factor

Trajectory No.	ME, deg	RMS, deg	IB, deg	
1	0.96	0.94	−1.15	3.18
2	0.57	1.02	−1.71	2.67
3	0.46	0.80	−1.38	2.27
4	0.82	0.99	−1.33	3.11
5	0.90	1.03	−1.34	3.18
6	0.99	1.07	−1.58	3.33

According to the simulation results for the available reference trajectories, the error in roll angle estimation in deterministic formulation and steady-state filter operation did not exceed 0.7°.

4. CONCLUSIONS

The proposed algorithm is used to estimate the roll angle of a spinning vehicle following a ballistic trajectory based on gyroscope data. From the simulation results for the available reference trajectories, the root-mean square deviation for the roll angle error did not exceed 1.07°. This is a good result for an autonomous attitude control system onboard a spinning vehicle based on medium-accuracy inertial sensors.

CONFLICT OF INTEREST

The authors of this work declare that they have no conflicts of interest.

REFERENCES

1. Vodicheva, L., Alievskaya, E., Koksharov, E., and Parysheva, Yu., Improving the accuracy of angular rate determination for spinning vehicles, *Gyroscopy and Navigation*, 2012, vol. 3, no. 3, pp. 159–167. https://doi.org/10.1134/S2075108712030091

2. Zhbanov, Yu.K., Klimov, D.M., Alekhova, E.Yu., Petelin, V.L., Slezkin, L. N., and Tereshkin, A.I., Scale factor correction of a strapdown angular rate sensor of a fast rotating object, *Gyroscopy and Navigation*, 2012, vol. 3, no. 4, pp. 275–278. https://doi.org/10.1134/S2075108712040128

3. Zhaowei Deng, Qiang Shen, Zilong Deng, and Jisi Cheng, Real-time estimation for roll angle of spinning projectile based on phase-locked loop on signals from single-axis magnetometer, *Sensors*, 2019, vol. 19, 839, https://doi.org/10.3390/s19040839.

4. Emel'yantsev, G. I., Stepanov, A.P., and Blazhnov, B.A., Attitude determination by INS/GNSS system aided by phase and magnetometer measurements for spinning vehicles, *Gyroscopy and Navigation*, 2014, vol. 5, no. 4, pp. 203–210. https://doi.org/10.1134/S207510871404004X

5. Hui Zhao, Zhong Su, Qing Li, Fuchao Liu, and Ning Liu, Real-time attitude propagation algorithm for high spinning flying bodies, *Measurement*, 2021, vol. 177, pp. 109–260. https://doi.org/10.1016/j.measurement.2021.109260

6. Shuangbiao Zhang, Zhong Su, and Xingcheng Li, Re-al-time angular motion decoupling and attitude updating method of spinning bodies assisted by satellite navigation data, *IEEE Access*, 2019, vol. 7. https://doi.org/10.1109/ACCESS.2019.2960602.

7. Hepner, D.J. and Harkins, T.E., Determining inertial orientation of a spinning body with body-fixed sensors, Army Research Laboratory, ARL-TR-2313, Jan. 2001.

8. Rogers, J. and Costello, M., A low-cost orientation estimator for smart projectiles using magnetometers and thermopiles, *Navigation*, March 2012, vol. 59, no. 1, pp. 9–24. https://doi.org/10.1002/navi.5

9. Fuchao Liu, Zhong Su, Hui Zhao, Qing Li, and Chao Li, Attitude measurement for high-spinning projectile with a hollow MEMS IMU consisting of multiple accelerometers and gyros, *Sensors*, 2019, vol. 19, no. 8, 1799. https://doi.org/10.3390/s19081799

10. Emel'yantsev, G. I., Nesenyuk, L.P., Blazhnov, B.A., Korotkov, A.N., and Stepanov, A.P., Design features of integrated INS/GNSS system for the objects following the initial ballistic trajectory, *Giroskopiya i navigatsiya*, 2009, no. 1, pp. 9–21.

11. Likhosherst, V.V. and Shvedov, A.P., Determining the angular motion parameters of spinning vehicles, Informatsionnye resursy, sistemy i tekhnologii, 2014, no. 3, *Proceedings of the 6th International Scientific and Practical Conference Informatsionnye tekhnologii v nauke, obrazovanii i proizvodstve* (Information Technologies in Science, Education, and Production).

12. Seregin, S.I., Attitude determination algorithm for spinning vehicles, *Trudy MAI*, 2013, no. 63.

13. Raspopov, V.Ya., Strapdown inertial navigation system for rotating flying vehicles, 20th St. Petersburg International *Conference on Integrated navigation Systems*, 2013.

14. Matveev, V.V., Data measurement attitude determination, stabilization, and navigation systems on Coriolis vibratory gyroscopes, D.Sci. *dissertation*, Tula, 2020.

15. Jiang Pan, Wang Guochen, Zhang Ya, Zhang Lin, Fan Shiwei, and Xu Dingjie, An improved attitude compensation algorithm in high dynamic environment, *IEEE Sensors Journal*, 2020, vol. 20, no. 1, pp. 306–317.

16. Recchia, T., Projectile velocity estimation using aerodynamics and accelerometer measurements: A Kalman filter approach, *Technical Report ARMET-TR-10010*, U.S. Army Armament Research, New Jersey, 2010.

17. Fairfax, L.D. and Fresconi, F.E., Cost-efficient state estimation for precision projectiles, *49th AIAA Aerospace Sciences Meeting including the New Horizons Forum and Aerospace Exposition*, 2011.

18. Bogdanov, M.B. and Savel'ev, V.V., Mathematical model of angular and linear coordinates of a small-sized guided aircraft with short flight time following the initial ballistic trajectory, *Izvestiya Tul'skogo gosudartvennogo universiteta. Tekhnicheskie nauki*, 2013, no. 11, pp. 8–24.

19. Lucia, D.J., Estimation of the local vertical state for guided munition shell with an embedded GPS/micromechanical inertial navigation system, *M.Sc. Thesis*, Massachusetts Institute of Technology, May 1995.

20. Hee Young Park, Kwang Jin Kim, Jang Gyu Lee, and Chan Gook Park, Roll angle estimation for smart munitions, *IFAC Proceedings Volumes*, 2007, vol. 40, no. 7, pp. 49–54.

21. Babichev, V.I., Gusev, A.V., Morozov, V.I., Shigin, A.V., Rabinovich, V.I., Dolgova, T.S., and Akulinin, S.I., A method to estimate the roll angle of a strapdown inertial navigation system of a spinning artillery projectile, RU *patent RU* (11) 2 584 400(13) C1, 2016.

22. Lindquist, E. and Kreichauf, R.D., Apparatus and appertaining method for upfinding in spinning projectiles using a phase-lock-loop or correlator mechanism, *Patent US* 7,395,987 B2, Jul. 8, 2008.

23. Kreichauf, R.D. and Lindquist, E., Estimation of the roll angle in a spinning guided munition shell, *IEEE/ION Position, Location, And Navigation Symposium*, 2006, https://doi.org/10.1109/PLANS.2006.1650580.

24. Yang Qifan, Wang Jiang, Fan Shipeng, Bai Chan, Zhou Yongjia, and Hu Shaoyong, In-flight alignment method of guided projectile roll angle based on trajectory bending angular velocity single vector, *Acta Armamentarii*, 2023, vol. 44, no. 2. https://doi.org/10.12382/bgxb.2021.0707